ARTICLE

Large-scale and flexible circularly polarized room temperature phosphorescence with a high dissymmetry factor and chiral sensing

Kunfeng Jin,[1] Chunchun Yin,[1] Jingxuan You,[1] Huailing Diao,[1] Jinfeng Wang,[2] Kunkun Zhu,[2] Jun Zhang,[1] and Jinming Zhang[1,*]

*Correspondence: zhjm@iccas.ac.cn

Received: May 27, 2024; Accepted: September 25, 2024; Published Online: October 16, 2024; https://doi.org/10.59717/j.xinn-mater.2024.100096

GRAPHICAL ABSTRACT

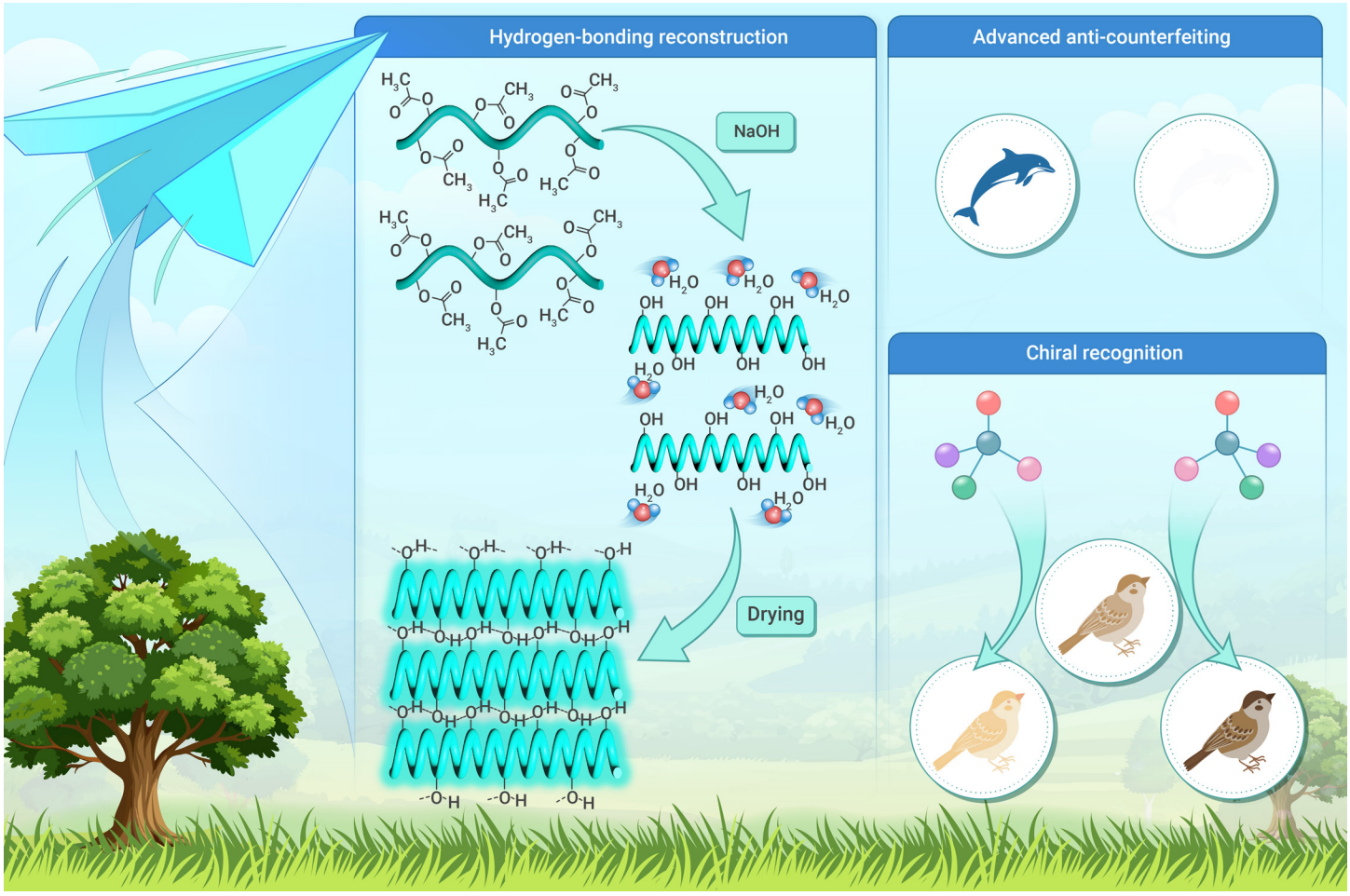

PUBLIC SUMMARY

- To amplify chirality by the reconstruction of hydrogen-bonding interactions in cellulose.
- A scale-up process to produce circularly polarized room-temperature phosphorescent (CP-RTP) materials.
- The gabs and glum of CP-RTP materials were as high as 0.48 and 0.16, respectively.
- CP-RTP materials showed a visual recognition performance to many enantiomers.

ARTICLE

www.the-innovation.org/materials

Large-scale and flexible circularly polarized room temperature phosphorescence with a high dissymmetry factor and chiral sensing

Kunfeng Jin,[1] Chunchun Yin,[1] Jingxuan You,[1] Huailing Diao,[1] Jinfeng Wang,[2] Kunkun Zhu,[2] Jun Zhang,[1] and Jinming Zhang[1,*]

[1]CAS Key Laboratory of Engineering Plastics, Institute of Chemistry, Chinese Academy of Sciences (CAS), Beijing 100190, China

[2]National Local Joint Laboratory for Advanced Textile Processing and Clean Production, Wuhan Textile University, Wuhan 430200, China

*Correspondence: zhjm@iccas.ac.cn

Received: May 27, 2024; Accepted: September 25, 2024; Published Online: October 16, 2024; https://doi.org/10.59717/j.xinn-mater.2024.100096

Citation: Jin K., Yin C., You J., et al., (2024). Large-scale and flexible circularly polarized room temperature phosphorescence with a high dissymmetry factor and chiral sensing. The Innovation Materials **2(4)**: 100096.

Circularly polarized luminescence (CPL) materials have attracted great attention because of their rich optical information and excellent sensitivity. However, the strategy to prepare CPL materials with a high dissymmetry factor (*g*) is still limited. Herein, we demonstrate a facile route to scale up the fabrication of circularly polarized organic room-temperature phosphorescent (CP-RTP) materials with a high *g* value, outstanding flexibility and complete biodegradability, via the reconstruction and enhancement of hydrogen-bonding interactions of cellulose. The absorption dissymmetry factor (g_{abs}) and luminescence dissymmetry factor (g_{lum}) of the CP-RTP materials are as high as 0.48 and 0.16, respectively, which are one or two orders of magnitude larger than previous records. These cellulose-based CP-RTP materials have full-color emission, and can be processed into different format. In particular, the CP-RTP materials exhibit chiral recognition performance in an instrument-free visual mode. They give a change of RTP performance once meeting different enantiomers, including lysine, histidine, cysteine, 2-chloromandelic acid, and 1-(2-naphthyl) ethanol. The novel strategy and new CP-RTP materials could promote the enrichment and practical applications of CPL materials.

INTRODUCTION

Circularly polarized luminescence (CPL) materials have broad application prospects in 3D displays, optical devices, bio-imaging, anti-counterfeiting, information storage and asymmetric synthesis, owing to their rich optical information and excellent sensitivity.[1-5] Traditionally, CPL can be achieved by using a linear polarizer and a quarter-wave plate. However, this method requires complex optical system, and causes the energy loss during the plate transition process. Alternatively, CPL materials have been developed to generate directly circularly polarized light, including CPL-active chiral molecules,[6-10] aggregation-induced emission (AIE) aggregates,[11-14] metal-ligand coordination compounds,[15-18] supramolecular assemblies,[19-22] liquid crystals,[23-27] and polymers.[28-30] For example, Nie et al. prepared a series of Zn-L-Histidine complexes with color-tunable circularly polarized room temperature phosphorescence (CP-RTP).[31] Du et al. have reported a solution-interface assembly strategy to fabricate hierarchically self-assembled helical microtoroids with circularly polarized fluorescence (CPF) performance.[19] Ma et al. mixed a series of chiral small molecular fluorophores with an optically inactive helical polymer to prepare multicolor CPL-active films.[32] However, practical applications for most of the reported CPL materials are limited due to their low luminescence dissymmetry factor (g_{lum}) of only 10^{-3}-10^{-2}. Recently, the CPL materials with a high g_{lum} value (> 0.10) have been reported using a liquid-crystal strategy. Liu et al. fabricated CP-RTP materials with a bilayer architecture by adding a small amount of RTP polymers into the liquid crystal system, and obtained bright and stable CPL materials with a high $|g_{lum}|$ of 1.49.[33] However, due to the internal filtering effect of the liquid crystal phase, the resultant CPL materials lose more than half of the energy.[24] In addition, liquid-crystal strategy has many restrictions for scaling up the preparation of CPL materials, such as the poor uniformity, time and energy consumption, high cost and low environmental friendliness. Therefore, there is still a demand to develop new methods to scale up the preparation of CPL materials with a high g_{lum} value, which would promote the enrichment and practical applications of CPL materials.

Phosphorescence is originated from triple excitons to the ground state (S_0) by radiative decay, and has the advantages of large Stokes shift, long lifetime, and long emission time. These characteristics enable CP-RTP materials to be used in a wide range of applications such as advanced data security, optoelectronic materials, and photodynamic therapy.[33-37] Zhang et al. constructed a pair of linear axially chiral conjugated polymers in a facile manner with ultralong afterglow of 33 s and g_{lum} value of 0.01.[35] Huang et al. doped bidibenzofuran compound into poly(vinyl alcohol) (PVA), which exhibited strong CP-RTP with RTP efficiency of 14.8%, g_{lum} value of 0.12, and lifetime of 0.56 s.[36] Chen et al. designed and incubated a pair of chiral organic ionic crystals, terephtalic (R/S)-phenylethyamine (TPA-(R/S)-PEA), which generated CP-RTP with lifetime up to 862 ms and g_{lum} value up to 0.02.[37] However, the low g_{lum} values limit practical application of CP-RTP materials.

Polymers are great candidates for preparing CPL materials owing to their excellent processability, mechanical properties, flexibility and stability.[34] Huang et al. dispersed a chiral helical polyacetylene into a poly(methyl methacrylate) (PMMA) matrix to produce a photoinduced CP-RTP material with an absorption dissymmetry factor (g_{abs}) and g_{lum} of 0.029 and 0.019, respectively.[38] Gu et al. synthesized chiral binaphthalene and further polymerized the chiral monomer to obtain CP-RTP materials with a lifetime of 680 ms and a g_{lum} value of 0.0094.[39] So far, polymer-based CPL materials still suffer from complicated synthesis, low g_{lum} value, poor luminescence efficiency, and low biodegradability. Natural polymers have also been used to fabricate the CPL materials. Xu et al. used cellulose nanocrystals as the raw materials to obtain cellulose photonic crystal films with an absorption of left circularly polarized light and an emission of right circularly polarized light, via an evaporation-induced self-assembly process.[40] However, the preparation process is time-consuming and difficult to scale up the process. Guo et al. embedded fluorenes into cellulose triacetate (CTA) and cellulose acetate butyrate (CAB) films, which showed a clear CPL with a g_{lum} value of 10^{-3}.[41] It is still a challenge to obtain polymer-based high-performance CPL materials through a simple, efficient and easy-to-scale strategy.

In this work, we report a new principle to construct and amplify chirality via reconstruction and enhancement of hydrogen-bonding interactions in cellulose chains. Based on this principle, a scale-up and continuous process was developed to produce CP-RTP materials with high *g* value, large area, excellent mechanical property, tunable colors and complete biodegradation. The g_{abs} and g_{lum} of the obtained CP-RTP materials were as high as 0.48 and 0.16, respectively. It is expected that this cellulose-based CP-RTP materials have great potential application in optical devices, anti-counterfeiting and visual sensing.

MATERIALS AND METHODS

Materials

Cellulose acetate was supplied by Sichuan Push Acetati Co., Ltd. N,N-dimethylformamide (DMF), trichloromethane, tetrahydrofuran (THF) and methanol (MeOH) were chromatographic grade and obtained from Concord Technology (Tianjin) Co., Ltd. Sodium hydroxide (NaOH) was purchased from Sinopharm Chemical Reagent Co., Ltd. Rhodamine 110 (Rh110), Rhodamine 123 (Rh123) and Rhodamine 6G (Rh6G) were purchased from J&K Scientific. Rhodamine B (RhB) was obtained from TCI Development Co., Ltd. Sulforhodamine 101 (Rh101) was purchased from Acros Organics. 1-Allyl-3-methylimidazolium chloride (AmimCl) was provided by Shangdong Henglian New Materials Co., Ltd. Dimethylsulfoxide-d_6 (DMSO-d_6, for NMR, 99.8 atom% D, with 0.03% (V/V) TMS) and all enantiomers were purchased from Beijing InnoChem Science & Technology Co., Ltd.

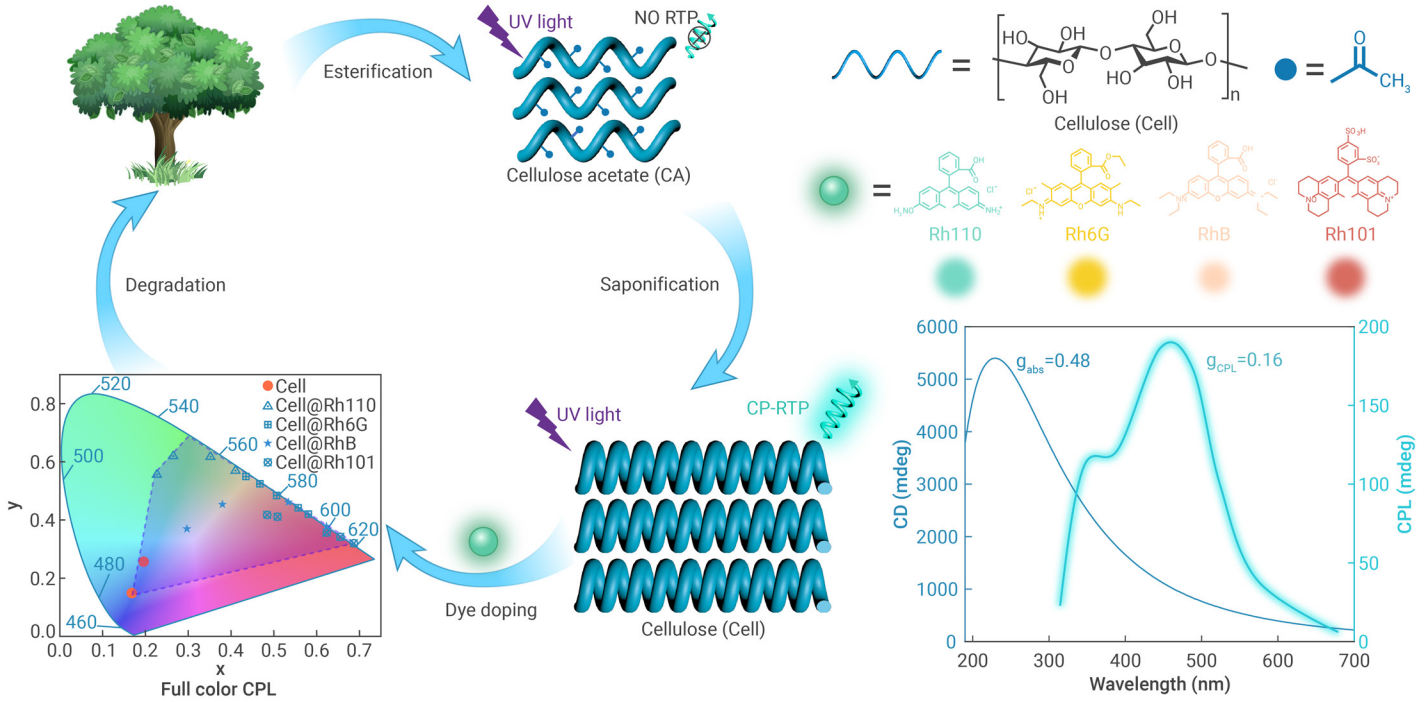

Figure 1. Schematic illustration of full-color CPL materials with high *g* value from natural cellulose.

Preparation of CA film

DMF was added into CA in a two-necked flask under stirring at 80 ℃ to obtain a CA/DMF solution with a concentration of 15-20 wt%. The CA/DMF solution was spread out on the glass plate by a scraping process. The solvent was evaporated at 40 ℃ to obtain the CA film.

Preparation of Cellulose (Cell) film

The CA film was soaked in NaOH solution (0.02 M-6 M) and was treated at 40℃ for 6 h to obtain Cell/NaOH hydrogel. Then, half-volume of NaOH solution was removed, and the same volume of ultrapure water was slowly added. This process was repeated until the pH value reached around 7.0 to obtain the Cell hydrogel. Finally, the hydrogel was dried in air at room temperature for 12 h, and then dried in vacuum at 80℃ for 8 h to obtain the Cell film.

Preparation of Cell@Rhs films

Cell hydrogels were immersed in methanol to obtain Cell methanol gels. The Cell methanol gels were soaked in Rhs/MeOH solutions (0.05-10 mg/mL) for 12 h. Subsequently, the above gels were placed in water to obtain Cell@Rhs hydrogels. The Cell@Rhs hydrogels were dried in air at room temperature for 12 h, and then dried in vacuum at 80℃ for 8 h to obtain Cell@Rhs films.

Preparation of Cell fibers

CA/acetone solution was used to produce CA fibers by a dry spinning process. Subsequently, the CA fibers were treated with NaOH solution (0.2 M), washed with water and freeze-dried to obtain cellulose fibers.

Preparation of Cell aerogel

The tows or films of CA, were treated with NaOH solution (2 M), washed with water and freeze-dried to obtain cellulose aerogels.

Degradation test

A 1.5 cm × 1.5 cm film of CA or cellulose was buried in soil. The film was taken out to observe its shape and record its weight at certain time intervals.

Characterization

^{13}C-NMR spectrum was obtained on a Bruker AV400 NMR spectrometer by dissolving CA in DMSO-d_6 with TMS as the internal standard. Solid-state ^{13}C-NMR spectrum was measured on a Bruker NEO 600 WB spectrometer operating at 150 MHz for ^{13}C using cross polarization and magic angle spinning (CP/MAS). Fourier transform infrared (FTIR) spectrum was recorded on a Nicolet 6700 (Thermal Fisher) spectrometer. X-ray diffraction (XRD) pattern was recorded in the angular range of 4-40° (*2θ*) with a scanning speed of 5 °/min by using an X-ray diffractometer (PANalytical, Netherlands). Circular dichroism (CD) spectrum and dissymmetric factor (g_{abs}) were obtained on a JASCO J-1500 spectrometer at 200 nm/min. Circularly polarized luminescence (CPL) spectrum and dissymmetric factor (g_{lum}) were obtained on a JASCO CPL-300 spectrometer at 200 nm/min. Fluorescence and phosphorescence spectra were recorded with a Hitachi F-7000 fluorescence spectrophotometer. Time-resolved decay spectrum was obtained on an Edinburgh FLS980 spectrophotometer equipped with a microsecond flash. Fluorescence and phosphorescence photographs were taken by a Sony α7 camera. Scanning electron microscopy (SEM) was carried out on a Hitachi SU8020 instrument with an accelerating voltage of 5 kV. Mechanical properties were tested on a universal tensile machine. The films were cut into 10 mm × 50 mm rectangular specimens. The tensile test was carried out at a tensile rate of 1 mm/min with a gauge length of 20 mm.

RESULTS AND DISCUSSION

Preparation of CP-RTP materials

Natural cellulose and its derivatives were selected as the raw materials. As the most abundant biopolymer in nature, cellulose has many advantages, such as bio-renewability, complete biodegradability, and excellent biocompatibility.[42-44] In particular, cellulose chain can form a helical structure, because it is made up of glucose units linked by β-(1,4) glycosidic bonds. Moreover, large numbers of hydroxyl groups are periodically distributed on the cellulose molecular chain. After chemical modification, various groups can be introduced into the cellulose side chain to obtain functional cellulose derivatives.[45-47] Cellulose acetate (CA) is the simplest cellulose derivative with excellent processability and formability, thus being applied in the fields of apparel, pharmaceuticals, tobacco, separations, and printing.[48-50] CA does not possess room temperature phosphorescence (RTP) property (Figure 1). When CA was saponified to remove the acetyl group, the resulting cellulose exhibited excellent CP-RTP performance. The g_{abs} and g_{lum} were as high as 0.48 and 0.16, respectively, which were much higher than those of previously reported CPL materials (g_{lum} = 10^{-3}-10^{-2}). After doping rhodamines (Rhs) into the cellulose film, the obtained materials not only showed full-color long-lived afterglow, but also exhibited CPL performance, owing to the chiral transfer

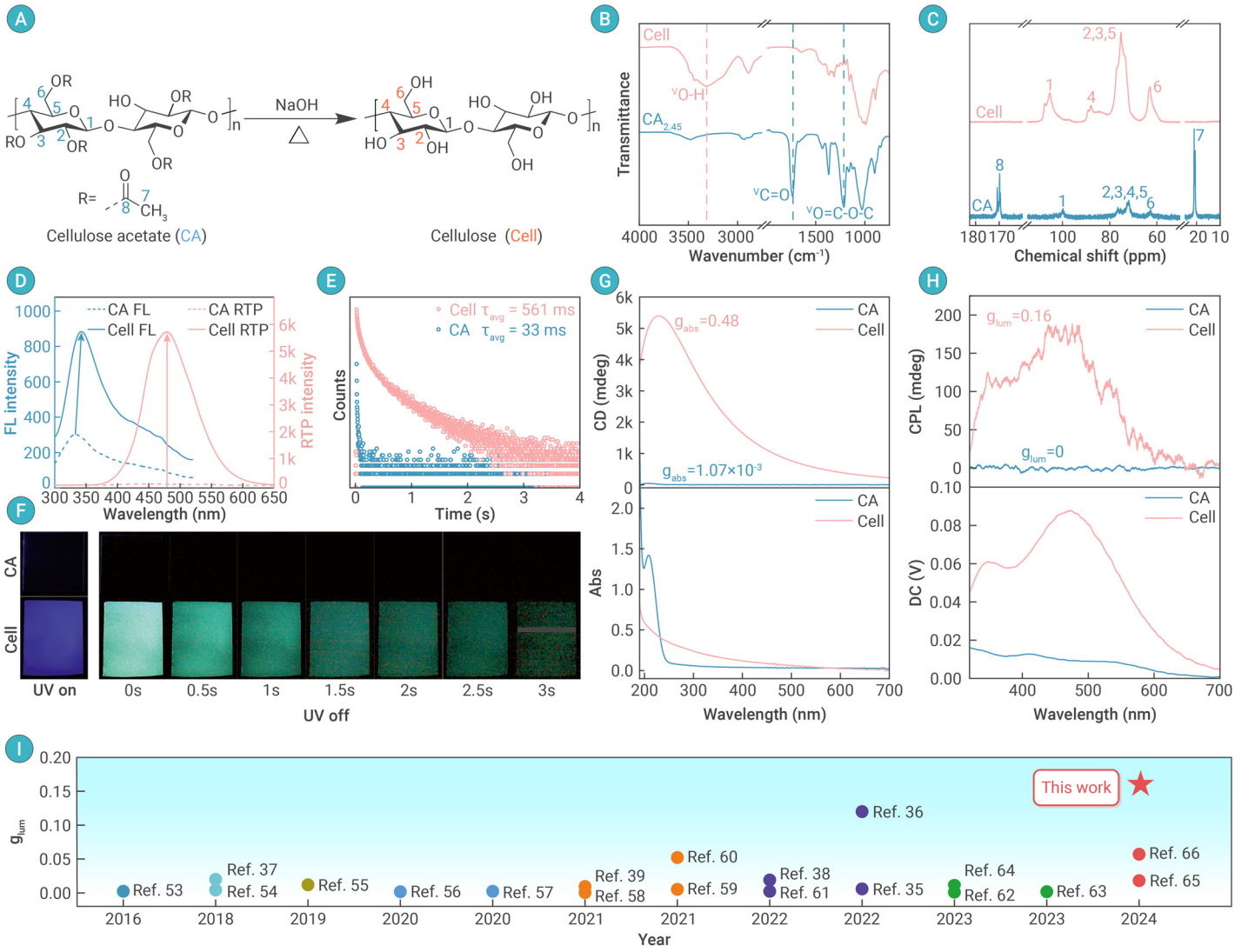

Figure 2. Preparation and properties of cellulose-based CP-RTP materials (A) Synthetic route, (B) FTIR spectra, (C) NMR spectra, (D) fluorescence and phosphorescence spectra, (E) phosphorescence lifetime, (F) fluorescence and phosphorescence photographs, (G) CD spectra, and (H) CPL spectra of CA and cellulose (Cell). (I) Comparison of g_{lum} values of CP-RTP materials obtained using non-liquid-crystal method from literatures.

from cellulose to Rhs (Figure 1). In addition, the as-prepared CPL materials contain mainly cellulose, which enables these materials biodegradable in soil, realizing a green recycling process of "originating from nature and returning to nature" (Figure 1).

CA undergoes a saponification process to remove the acetyl groups and obtain cellulose in alkaline solution (Figure 2A). As for CA, the peaks at 1735 cm^{-1} and 1210 cm^{-1} in the FTIR spectrum are assigned to C=O stretching vibration peak and (O=C)-O-C stretching vibration peak, respectively. These peaks completely disappeared after NaOH treatment, accompanying with the great increase of the O-H stretching vibration peak at 3320 cm^{-1} (Figure 2B). ^{13}C-NMR spectra showed that the peaks of C=O at 170 ppm and CH_3 at 21 ppm completely disappeared after NaOH treatment (Figure 2C). XRD patterns showed that CA was amorphous (Figure S1). After NaOH treatment, the obtained cellulose material was a typical cellulose II with a crystallinity of 79.3% (Figure S1). These results confirmed the successful removal of acetyl groups after the saponification process of CA.

The fluorescence emission of CA was very weak, and almost no phosphorescence emission was observed at room temperature (Figures 2D-F). After NaOH treatment, the resulting cellulose material showed both fluorescence emission (343 nm) and phosphorescence emission (478 nm) (Figures 2D-F), achieving a phosphorescence lifetime of 561 ms (Figure 2E & Table S1). This is because cellulose contains a large number of O-O clusters which act as luminescent centers.[51,52] Meanwhile, cellulose has strong intramolecular and intermolecular hydrogen-bonding interactions, which prevent the motion of chains and groups to inhibit non-radiative relaxation, thus promoting the fluorescence and phosphorescence emission. By contrast, CA has a high content of acetyl group and a low content of hydroxyl group, which not only reduces the O-O clusters, but also severely disturbs the hydrogen-bonding interactions. Therefore, very weak fluorescence and phosphorescence are observed for CA. The fluorescence and phosphorescence emission of cellulose exhibited an obvious characteristic of cluster-induced emission, which indicated the fluorescence and phosphorescence emission were excitation-dependence. The emission wavelength gradually red-shifted as the excitation wavelength increased (Figure S2). The obtained cellulose film showed purple fluorescence and cyan phosphorescence at 280 nm excitation, while emitted blue fluorescence and green phosphorescence at 365 nm excitation. These phenomena indicate the presence of multiple cluster luminescence centers in the as-prepared cellulose material.

CD spectrum showed that CA had a low g_{abs} of 1.07 × 10^{-3} (Figure 2G), and the CPL spectrum showed that CA had not CPL property (Figure 2H). These results indicated that the CA film had a negligible chirality. After NaOH treatment, the obtained cellulose film exhibited a strong chirality with a high g_{abs} of 0.48 (Figures 2H & S4). CPL spectra showed that the fluorescence emission peak (347 nm) and phosphorescence emission peak (465 nm) had circularly polarized property with a high g_{lum} of 0.16, which is the highest value among all the reported materials prepared using non-liquid-crystal methods (Figure 2I).

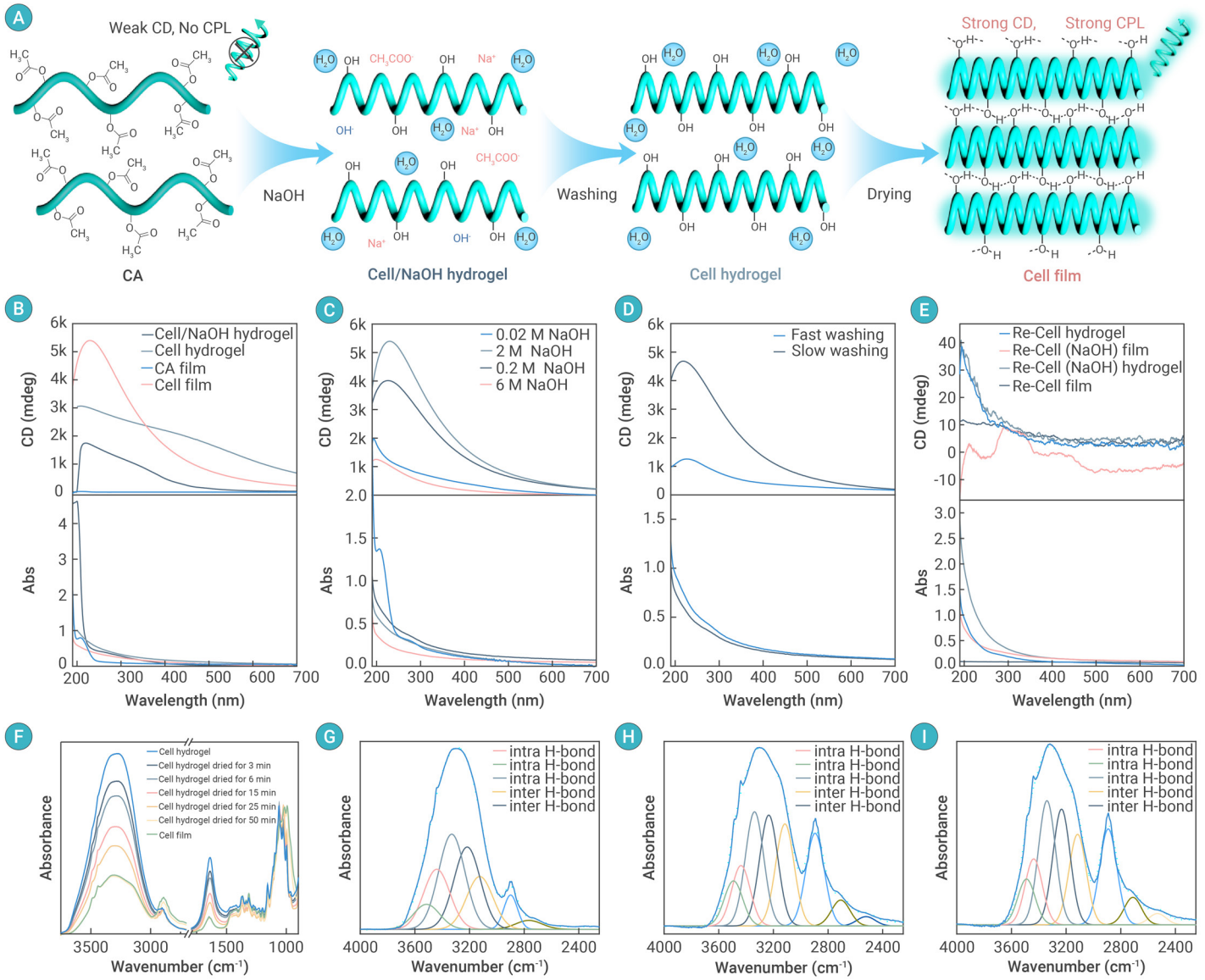

Figure 3. Mechanism of cellulose-based CP-RTP materials (A) Schematic diagram of the mechanism. (B) CD spectra of CA film, Cell/NaOH hydrogel, Cell hydrogel and Cell film. (C) Effect of the NaOH concentration on the CD spectra of cellulose-based CP-RTP materials. (D) Effect of the washing method on the CD spectra of cellulose-based CP-RTP materials. (E) CD spectra of dissolving-regenerated cellulose (Re-Cell) hydrogel and film obtained from cellulose/AmimCl solution. (F) FTIR spectra of cellulose hydrogels and cellulose film. (G) FTIR peak fitting of cellulose hydrogel dried for 25 min in air. (H) FTIR peak fitting of cellulose hydrogel dried for 50 min in air. (I) FTIR peak fitting of cellulose film.

Mechanism of CP-RTP materials

The chirality change of CA after the deacetylation process was investigated in detail (Figure 3). CA film exhibited weak chirality with a positive Cotton effect (Figures 3B & S3). CD value of CA film was only 45 mdeg at 209 nm, and the g_{abs} was only 1.07 × 10^{-3}. After NaOH treatment, the acetyl groups detached from the cellulose chains, leading to exposure of hydroxyl groups and formation of a large amount of free space around the cellulose chains. As a result, the intrachain hydrogen-bonding interactions of cellulose were greatly enhanced. This was confirmed by the appearance of the O-H peaks at 3514 cm^{-1}, 3440 cm^{-1} and 3328 cm^{-1} in FTIR spectrum (Figures 3F-G), corresponding to the intrachain hydrogen-bonding interactions of cellulose. Meanwhile, the greatly increased free space around the cellulose chain, facilitating cellulose chains to form chiral helical structure. The CD and g_{abs} values increased to 1.75 × 10^3 mdeg and 0.20, respectively (Figure 3B). Subsequently, the free OH^-, CH_3COO^- and Na^+ ions were displaced with water. Chirality of the treated CA film was further improved with increased CD and g_{abs} values of 3.06 × 10^3 mdeg and 0.45, respectively. This is because free OH^-, CH_3COO^- and Na^+ ions can form strong interactions with the hydroxyl groups of cellulose, weakening the intrachain hydrogen-bonding interactions. As the removal of OH^-, CH_3COO^- and Na^+ ions, the intrachain hydrogen-bonding interactions in cellulose were further enhanced, leading to improve chiral characteristic. Finally, the drying process removed water from the cellulose hydrogel, which led to further enhancement of intrachain (O-H peaks at 3494cm^{-1}、 3438 cm^{-1} and 3328 cm^{-1}) and interchain (O-H peaks at 3234 cm^{-1} and 3116 cm^{-1}) hydrogen-bonding interactions (Figures 3H-I),[67-69] thus the cellulose film exhibited the strongest chiral characteristic among all the tested samples. The CD and g_{abs} values increased to 5.40 × 10^3 mdeg and 0.48, respectively. In brief, during the saponification process of CA, hydroxyl groups were released to restore intrachain hydrogen-bonding interactions of cellulose, resulting in the formation of a chiral helical structure (Figure 3A). The intrachain and interchain hydrogen-bonding interactions were further enhanced during the washing and drying steps, thus improving the chirality of the material. Based on the reconstruction and enhancement of hydrogen-bonding interactions in cellulose, chirality can be effectively constructed and amplified to obtain cellulose-based CP-RTP materials.

Chirality of the resulting cellulose materials varied with the NaOH concentration during the treatment, owing to the different deacetylation rate and the swollen degree of cellulose (Figures 3C & S5). When the NaOH concentration increased from 0.02 M to 2 M, the CD and g_{abs} values increased from 3.55 × 10^3 mdeg and 0.25 to 5.40 × 10^3 mdeg and 0.48, respectively. This is because

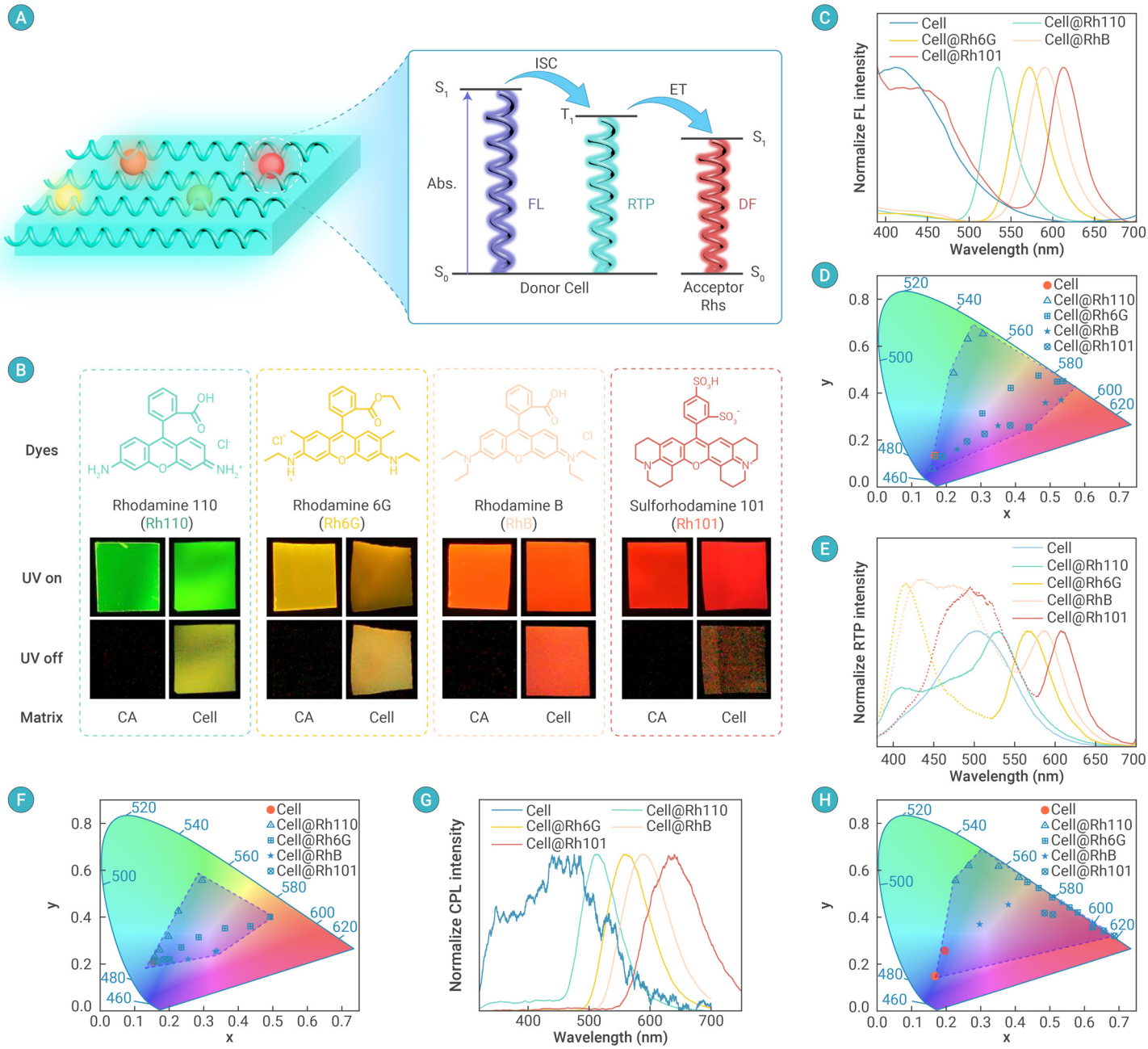

Figure 4. Preparation and performance of full-color CPL materials (A) Schematic of the mechanism of full-color CPL. (B) Fluorescence and phosphorescence photographs of full-color CPL materials, and the molecular structure of the Rhs used. (C) Full-color fluorescence spectra and (D) CIE color coordinates of Cell@Rhs. (E) Full-color phosphorescence spectra and (F) CIE color coordinates of Cell@Rhs. (G) Full-color CPL spectra and (H) CIE color coordinates of Cell@Rhs.

higher concentration NaOH solution resulted in faster deacetylation rate and higher swollen degree of cellulose. However, further increase of NaOH concentration to 6 M led to decreased CD and g_{abs} values of 1.26×10^3 mdeg and 0.14, respectively. This mainly attributed to increased amount of NaOH which could form strong interactions with the hydroxyl groups of cellulose, preventing the formation of intrachain hydrogen-bonding interactions in cellulose. In addition, the removal rate of free OH^-, CH_3COO^- and Na^+ ions also had an important effect on the chirality of cellulose film (Figures 3D & S6-S7). When Cell/NaOH hydrogel was directly immersed into water for a rapid removal of free ions, the CD and g_{abs} values of the resulting cellulose film were 1.55×10^3 mdeg and 0.072, respectively. When Cell/NaOH hydrogel was immersed into NaOH solutions with gradient concentrations, the CD and g_{abs} values of the resulting cellulose film were 4.68×10^3 mdeg and 0.32, respectively. Rapid solvent exchange rate made a sharp decrease of the swollen degree of cellulose, which is adverse to the change of cellulose chain conformation to form the chiral helical structure. Moreover, drying method also had a significant effect on the chirality of cellulose film (Figure S8). When the cellulose hydrogel was rapidly dried in a vacuum oven at 60℃, the CD and g_{abs} values of the cellulose film were 3.31×10^3 mdeg and 0.23, respectively. This is compared with an increase CD and g_{abs} values (3.73×10^3 mdeg and 0.32) for the cellulose film when the cellulose hydrogel was slowly dried at room temperature.

To further elucidate the mechanism, regenerated cellulose (Re-Cell) hydrogel and film were prepared by using 1-allyl-3-methylimidazolium chloride (AmimCl) ionic liquid as the solvent and water as the precipitant (Figure 3E). CD spectra showed that the Re-Cell hydrogel and Re-Cell film had almost no chirality and no chiral signal was observed even after treating with NaOH solution. These results suggest that the saponification process enabled the removal of acetyl groups and promoted the formation of large free space, which plays an essential role in the formation of the chiral helical structure of cellulose chains.

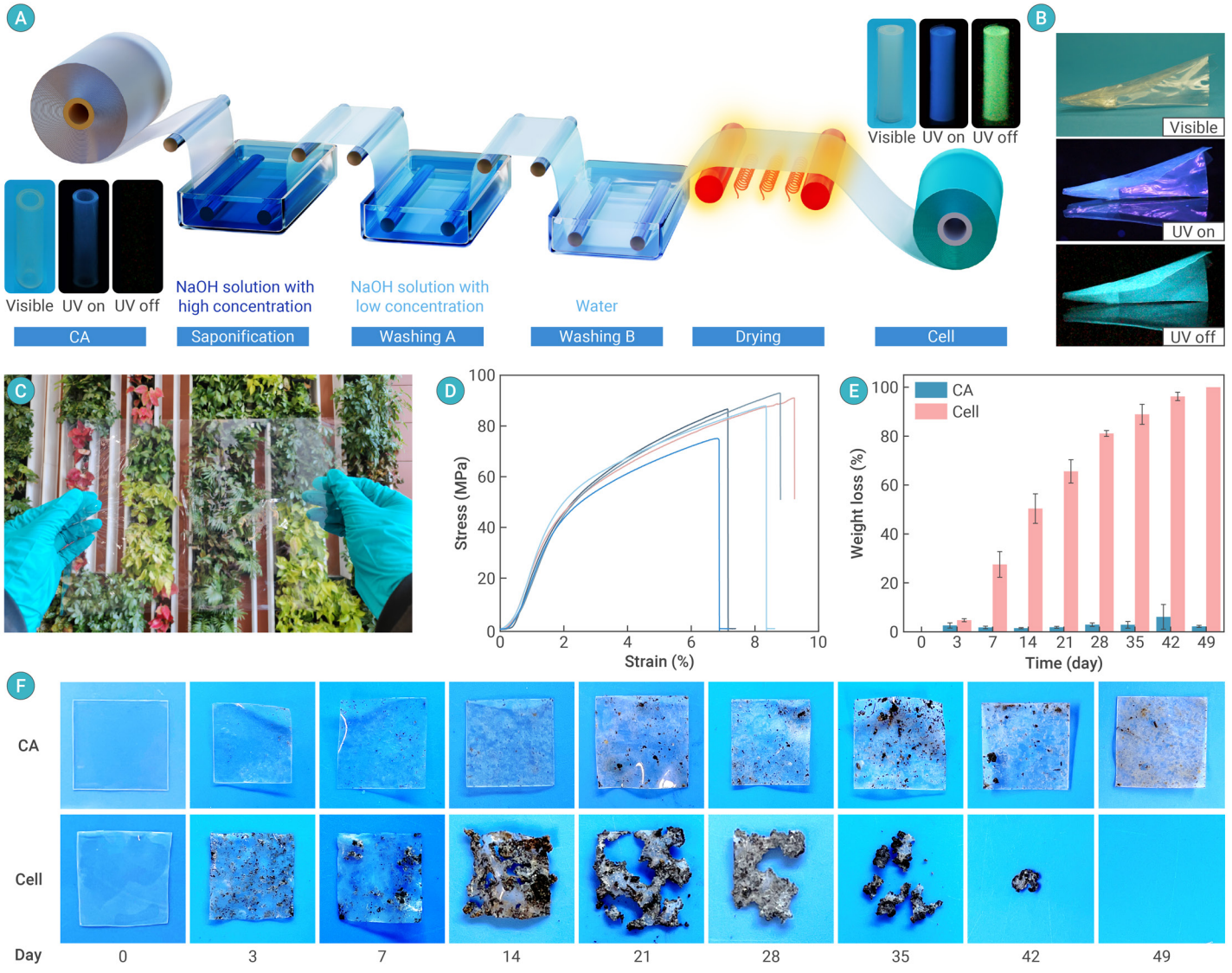

Figure 5. Large-scale preparation of full-color CPL films (A) Schematic diagram of continuous large-scale production of cellulose CP-RTP films. (B) Visible, fluorescence and phosphorescence photographs of an airplane folded with cellulose film. (C) Visible photograph of a large-size cellulose film. (D) Tensile curves of cellulose films. (E) Weight loss rate of CA and cellulose films in soil. (F) Photographs of the degradation process of CA and cellulose films in soil.

Full-color CPL materials

Cellulose CP-RTP film with a high *g* value was used as a substrate. After doping commercial rhodamines (Rhs) dyes, full-color long-lived CPL materials were obtained (Figures 4A-B). Fluorescence emission of the resulting materials ranged from 412 nm to 614 nm (Figure 4C), and the fluorescence colors changed from blue-violet (Cell), to green (Cell@Rh110), yellow (Cell@Rh6G), orange (Cell@RhB), and red (Cell@Rh101) (Figures 4B-D & S9-S13). The phosphorescent emission ranged from 467 nm to 609 nm (Figure 4E), and the phosphorescent colors changed from cyan (Cell), to green (Cell@Rh110), yellow (Cell@Rh6G), orange (Cell@RhB), and red (Cell@Rh101) (Figures 4B, E-F, S9-S14, & Table S2). Modulating the content of Rhs could finely regulate the fluorescent and phosphorescent properties of the resulting materials. The fluorescence and phosphorescence emission intensity of Cell decreased as increasing the content of Rhs (Figures S15-S17). Meanwhile, the phosphorescence lifetime of Cell at 478 nm (λ_{ex} = 270 nm) also decreased with the increase of Rhs content (Figure S18 & Table S3). These results demonstrate that the full color fluorescence emission and phosphorescence emission are achieved by T-S energy transfer between Cell and Rhs.[70,71]

The resulting cellulose@Rhs materials exhibited full-color CPL emission due to the chiral transfer effect (Figures 4G-H & S19-S22). The CD and CPL spectra showed the cellulose@Rhs films had strong chirality with g_{abs} as high as 0.30 and g_{lum} as high as 0.11 (Figure S19-S21). The wavelength of the CPL emission red-shifted from 465 nm (Cell) to 514 nm (Cell@Rh110), 560 nm (Cell@Rh6G), 586 nm (Cell@RhB), 630 nm (Cell@Rh101) (Figure 4G). Further modulation of the Rhs content could get a full-color CPL materials with a super-wide color gamut (Figure 4H).

Scale-up preparation and application of full-color CPL materials

CA has the excellent processability and formability. The CP-RTP could be easily fabricated into different material forms, including film, fiber, aerogel, 3D object and patterns via a continuous process of "solution processing, saponification, washing and drying" in a large scale (Figures 5-6). For example, large-size CP-RTP films (g_{lum} = 0.13) were obtained by using commercial CA film (Figure 5A). The CP-RTP film had excellent flexibility and could be folded repeatedly into various 3D objects, such as an "airplane" model (Figure 5B & S23). In addition, the CP-RTP film had a high transparency and excellent mechanical properties with a tensile strength of 86.8 ± 7.0 MPa and an elongation at break of 8.1 ± 1.0% (Figures 5C-D). Furthermore, the CP-RTP film was completely degradable in the natural environment (Figures 5E-F). More than 60% mass was achieved within 21 days in soil, and the material completely disappeared after 49 days. This CP-RTP material can be discarded directly after use without causing environmental pollution, realizing the green recycling process of "originating from nature and returning to

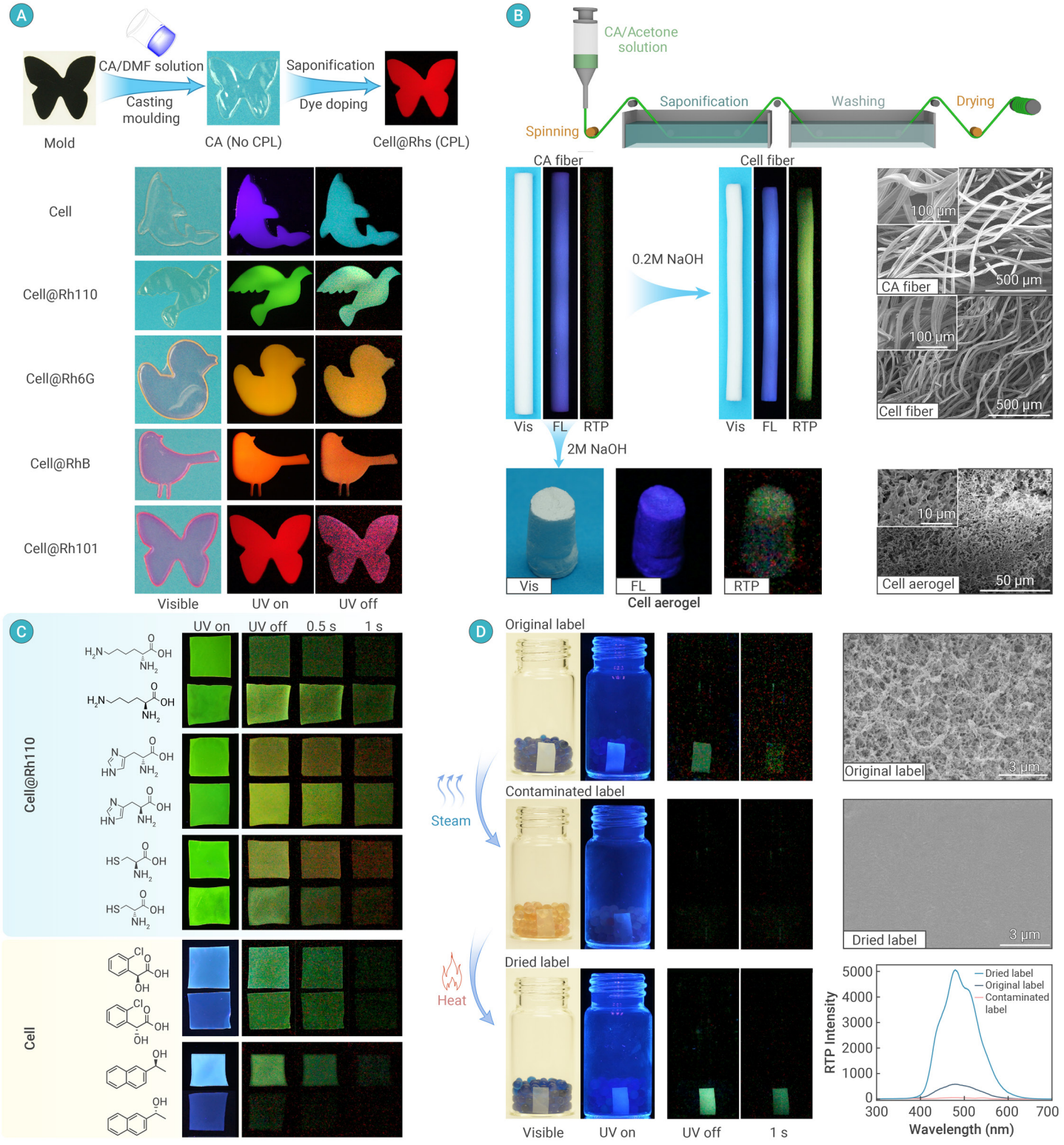

Figure 6. Large-scale preparation and application of full-color CPL materials (A) Cellulose-based full-color phosphorescent patterns. (B) Cellulose-based phosphorescent fibers and aerogel. (C) Visual identification of enantiomers. (D) Visual labels for irreversible moisture responsiveness.

nature". This environmentally-friendly CP-RTP material has great promising application in many fields, such as flexible 3D display and environmentally-friendly optical devices.

CA with designed patterns can be obtained by pouring CA/DMF solution into the mold followed by solvent evaporation. Subsequently, after a process of saponification, washing, doping and drying, full-color patterns with long-lived afterglow performance were obtained (Figure 6A). This makes the CA material a great candidature as environmentally-friendly phosphorescent anti-counterfeiting label. CA fibers produced by a dry spinning process were treated to obtain green phosphorescent fibers (Figure 6B). After treating commercial CA tows and films with 2M NaOH solution, cellulose aerogels with weak fluorescence and phosphorescence emission were obtained (Figure 6B).

Because of the high sensitivity, the as-prepared CP-RTP films and patterns could recognize many enantiomers in a visual mode, including lysine, histidine, cysteine, 2-chloromandelic acid, and 1-(2-naphthyl) ethanol (Figures 6C-

D & S24). For example, L-lysine extended the phosphorescence lifetime and brightened the phosphorescence emission of Cell and Cell@Rh110 films, while D-lysine had an opposite effect. When L-histidine was used, Cell@Rh110 showed a color change from yellow to yellowish green. The D-cysteine enabled Cell@Rh110 change color from yellow to green. After the addition of the S-1-(2-naphthyl) ethanol, Cell exhibited an obvious change of the fluorescence color and a quenching of the RTP. The addition of (S)-(+)-2-chloromandelic acid to Cell showed a similar phenomenon. In addition, the above cellulose aerogel exhibited irreversible humidity responsiveness (Figure 6D). It was used as the irreversible humidity label. The discoloration silica gel was used as the common humidity label. The initial cellulose aerogel had a weak phosphorescence, and the silica gel was blue. Once exposed to moisture, the silica gel turned into red. The silica gel restored blue after drying to remove water, while the cellulose label emitted brightly green phosphorescence. During this process, the loose structure of cellulose aerogel was transformed into a dense structure, enhancing the cellulose chain interactions and preventing the entry of oxygen and water. Thus, the phosphorescence performance significantly enhanced. This process cannot be restored to its original state. Therefore, the cellulose aerogel can be used as a visual and unfalsified label to monitor whether items have been exposed to a high-humidity environment, which is crucial for the storage of humidity-sensitive materials, such as food and medicine.

This novel and straight-forward strategy can be used to prepare various large-size CP-CRT materials with a high *g* value, excellent mechanical property, and complete biodegradation. The resultant cellulose-based CP-CRT materials exhibit great application prospects in the fields of 3D display, flexible optical devices, molecular recognition, environmental monitoring, information storage, anti-counterfeiting and encryption.

CONCLUSION

We demonstrated an effective strategy to construct and amplify chirality by controlling the reconstruction and enhancement of hydrogen-bonding interactions in cellulose. A scale-up and continuous process was successfully developed to produce CP-RTP materials with a high *g* value, large size, flexibility, excellent mechanical property, tunable colors and complete biodegradation. The CP-RTP materials could be easily processed into flexible films, fibers, aerogels, 3D objects and patterns with full-color emission. The g_{abs} and g_{lum} of the resulting materials were as high as 0.48 and 0.16, respectively, which were the highest value among all the reported materials obtained using non-liquid-crystal methods. The phosphorescence lifetime was as high as 561 ms. When CP-RTP was made into an aerogel, it exhibited an irreversible humidity responsiveness, making it a great candidature for an unforgeable tag to monitor the environment change and food freshness. Importantly, the CP-RTP materials showed a distinct change of RTP performance after the addition of different enantiomers, including lysine, histidine, cysteine, 2-chloromandelic acid, and 1-(2-naphthyl) ethanol. This work opens a new doorway to guide further design of advanced CP-RTP materials for a broad range of applications.

REFERENCES

1. Mayorga Burrezo, P., Jimenez, V.G., Blasi, D., et al. (2019). Organic free radicals as circularly polarized luminescence emitters. Angew. Chem. Int. Ed. **58**: 16282–16288. DOI: 10.1002/anie.201909398.
2. Sang, Y., Han, J., Zhao, T., et al. (2020). Circularly polarized luminescence in nanoassemblies: Generation, amplification, and application. Adv. Mater. **32**: e1900110. DOI: 10.1002/adma.201900110.
3. Gong, Z.-L., Zhu, X., Zhou, Z., et al. (2021). Frontiers in circularly polarized luminescence: molecular design, self-assembly, nanomaterials, and applications. Sci. China: Chem. **64**: 2060–2104. DOI: 10.1007/s11426-021-1146-6.
4. Zhang, Y., Yu, S., Han, B., et al. (2022). Circularly polarized luminescence in chiral materials. Matter **5**: 837–875. DOI: 10.1016/j.matt.2022.01.001.
5. Tang Z. (2023). Printable circularly polarized luminescence materials for advancing flexible 3D imaging. The Innovation Materials **1**: 100038. DOI: 10.59717/j.xinn-mater.2023.100038.
6. Qiu, Z., Ju, C.W., Frederic, L., et al. (2021). Amplification of dissymmetry factors in pi-extended [7]- and [9]helicenes. J. Am. Chem. Soc. **143**: 4661–4667. DOI: 10.1021/jacs.0c13197.
7. Takaishi, K., Matsumoto, T., Kawataka, M., et al. (2021). Circularly polarized luminescence liquids based on siloxybinaphthyls: Best binaphthyl dihedral angle in the excited state. Angew. Chem. Int. Ed. **60**: 9968–9972. DOI: 10.1002/anie.202101226.
8. Sun Y., Wang H., Liu S., et al., (2023). Paracyclophane-based bipolar near-ultraviolet emitters showing advanced circularly polarized luminescent properties. The Innovation Materials **1**: 100028. DOI: 10.59717/j.xinn-mater.2023.100028.
9. Lin, M., Bian, L., Chen, Q., et al. (2023). Cyclization of an achiral flipping panel to homochiral tubes exhibiting circularly polarized luminescence. Angew. Chem. Int. Ed. **62**: e202303035. DOI: 10.1002/anie.202303035.
10. Zhao, F., Zhao, J., Liu, H., et al. (2023). Synthesis of pi-conjugated chiral organoborane macrocycles with blue to near-infrared emissions and the diradical character of cations. J. Am. Chem. Soc. **145**: 10092–10103. DOI: 10.1021/jacs.3c00306.
11. Li, W.J., Gu, Q., Wang, X.Q., et al. (2021). AIE-active chiral [3]rotaxanes with switchable circularly polarized luminescence. Angew. Chem. Int. Ed. **60**: 9507–9515. DOI: 10.1002/anie.202100934.
12. Xia, Q., Meng, L., He, T., et al. (2021). Direct visualization of chiral amplification of chiral aggregation induced emission molecules in nematic liquid crystals. ACS Nano **15**: 4956–4966. DOI: 10.1021/acsnano.0c09802.
13. Garci, A., Abid, S., David, A.H.G., et al. (2022). Aggregation-induced emission and circularly polarized luminescence duality in tetracationic binaphthyl-based cyclophanes. Angew. Chem. Int. Ed. **61**: e202208679. DOI: 10.1002/anie.202208679.
14. Zhang, X., Liu, H., Zhuang, G., et al. (2022). An unexpected dual-emissive luminogen with tunable aggregation-induced emission and enhanced chiroptical property. Nat. Commun. **13**: 3543. DOI: 10.1038/s41467-022-31281-9.
15. Li, B., Li, Y., Chan, M.H., et al. (2021). Phosphorescent cyclometalated platinum(II) enantiomers with circularly polarized luminescence properties and their assembly behaviors. J. Am. Chem. Soc. **143**: 21676–21684. DOI: 10.1021/jacs.1c10943.
16. Kotova, O., O'Reilly, C., Barwich, S.T., et al. (2022). Lanthanide luminescence from supramolecular hydrogels consisting of bio-conjugated picolinic-acid-based guanosine quadruplexes. Chem **8**: 1395–1414. DOI: 10.1016/j.chempr.2022.01.015.
17. Willis, B.N., Schnable, D., Schley, N.D., and Ung, G. (2022). Spinolate lanthanide complexes for high circularly polarized luminescence metrics in the visible and near-infrared. J. Am. Chem. Soc. **144**: 22421–22425. DOI: 10.1021/jacs.2c10364.
18. Jin, Y., Peng, Q.C., Xie, J.W., et al. (2023). Photo-activated circularly polarized luminescence film based on aggregation-induced emission copper(I) cluster-assembled materials. Angew. Chem. Int. Ed. **62**: e202301000. DOI: 10.1002/anie.202301000.
19. Du, C., Li, Z., Zhu, X., et al. (2022). Hierarchically self-assembled homochiral helical microtoroids. Nat. Nanotechnol. **17**: 1294–1302. DOI: 10.1038/s41565-022-01234-w.
20. Feng, L.Z., Wang, J.J., Ma, T., et al. (2022). Biomimetic non-classical crystallization drives hierarchical structuring of efficient circularly polarized phosphors. Nat. Commun. **13**: 3339. DOI: 10.1038/s41467-022-30989-y.
21. Zhang, Y., Li, H., Geng, Z., et al. (2022). Dynamically stable and amplified circularly polarized excimer emission regulated by solvation of chiral co-assembly process. Nat. Commun. **13**: 4905. DOI: 10.1038/s41467-022-32714-1.
22. Geng, Z., Liu, Z., Li, H., et al. (2023). Inverted and amplified CP-EL behavior promoted by AIE-Active chiral co-Assembled helical nanofibers. Adv. Mater. **35**: e2209495. DOI: 10.1002/adma.202209495.
23. Hou, J., Toyoda, R., Meskers, S.C.J., and Feringa, B.L. (2022). Programming and dynamic control of the circular polarization of luminescence from an achiral fluorescent dye in a liquid crystal host by molecular motors. Angew. Chem. Int. Ed. **61**: e202206310. DOI: 10.1002/anie.202206310.
24. Liu, S., Liu, X., Wu, Y., et al. (2022). Circularly polarized perovskite luminescence with dissymmetry factor up to 1.9 by soft helix bilayer device. Matter **5**: 2319-2333. DOI: 10.1016/j.matt.2022.05.012.
25. Zhang, X., Xu, Y., Valenzuela, C., et al. (2022). Liquid crystal-templated chiral nanomaterials: from chiral plasmonics to circularly polarized luminescence. Light Sci. Appl. **11**: 223. DOI: 10.1038/s41377-022-00913-6.
26. Luo, Z.-W., Huang, A., Luo, H.-Y., et al. (2023). Regulating circularly polarized luminescent behavior of luminescent liquid crystalline polymers through resonance energy transfer. Macromolecules **56**: 2700–2708. DOI: 10.1021/acs.macromol.3c00002.
27. Wu, Y., Li, M., Zheng, Z.G., et al. (2023). Liquid crystal assembly for ultra-dissymmetric circularly polarized luminescence and beyond. J. Am. Chem. Soc. **145**: 12951–12966. DOI: 10.1021/jacs.3c01122.
28. Liu, W.-B., Xu, X.-H., Kang, S.-M., et al. (2021). Bottlebrush polymers carrying side chains on every backbone atom: controlled synthesis, polymerization-induced emission, and circularly polarized luminescence. Macromolecules **54**: 3158–3168. DOI: 10.1021/acs.macromol.1c00016.
29. Pan, M., Zhao, R., Zhao, B., et al. (2021). Two chirality transfer channels assist handedness inversion and amplification of circularly polarized luminescence in chiral helical polyacetylene thin films. Macromolecules **54**: 5043–5052. DOI: 10.1021/acs.macromol.1c00563.
30. Xu, L., Wang, C., Li, Y.X., et al. (2020). Crystallization-driven asymmetric helical assembly of conjugated block copolymers and the aggregation induced white-light emission and circularly polarized luminescence. Angew. Chem. Int. Ed. **59**: 16675–16682. DOI: 10.1002/anie.202006561.
31. Nie, F., Wang, K.Z., and Yan, D. (2023). Supramolecular glasses with color-tunable circularly polarized afterglow through evaporation-induced self-assembly of chiral metal-organic complexes. Nat. Commun. **14**: 1654. DOI: 10.1038/s41467-023-37331-0.
32. Ma, S., Zhao, B., and Deng, J. (2023). Helical polymer working as a chirality amplifier

to generate and modulate multicolor circularly polarized luminescence in small molecular fluorophore/polymer composite films. ACS Cent. Sci. **9**: 1409–1418. DOI: 10.1021/acscentsci.3c00122.
33. Liu, J., Song, Z.P., Wei, J., et al. (2024). Circularly polarized organic ultralong room-temperature phosphorescence with a high dissymmetry factor in chiral helical superstructures. Adv. Mater. **36**: e2306834. DOI: 10.1002/adma.202306834.
34. Zhong, H., Zhao, B., and Deng, J. (2023). Polymer - based circularly polarized luminescent materials. Adv. Opt. Mater. **11**: 2202787. DOI: 10.1002/adom.202202787.
35. Zhang, D.W., Li, M., and Chen, C.F. (2022). Linear axially chiral conjugated polymers exhibiting ultralong low-temperature phosphorescence and intense circularly polarized luminescence. Angew. Chem. Int. Ed. **61**: e202213130. DOI: 10.1002/anie.202213130.
36. Huang, W., Fu, C., Liang, Z., et al. (2022). Strong circularly-polarized room-temperature phosphorescence from a feasibly separable scaffold of bidibenzo[b,d]furan with locked axial chirality. Angew. Chem. Int. Ed. **61**: e202202977. DOI: 10.1002/anie.202202977.
37. Chen, W., Tian, Z., Li, Y., et al. (2018). Long-persistent circularly polarized phosphorescence from chiral organic ionic crystals. Chem.-Eur. J. **24**: 17444–17448. DOI: 10.1002/chem.201804342.
38. Huang, Z., He, Z., Ding, B., et al. (2022). Photoprogrammable circularly polarized phosphorescence switching of chiral helical polyacetylene thin films. Nat. Commun. **13**: 7841. DOI: 10.1038/s41467-022-35625-3.
39. Gu, L., Ye, W., Liang, X., et al. (2021). Circularly polarized organic room temperature phosphorescence from amorphous copolymers. J. Am. Chem. Soc. **143**: 18527–18535. DOI: 10.1021/jacs.1c08118.
40. Zheng, H., Li, W., Li, W., et al. (2018). Uncovering the circular polarization potential of chiral photonic cellulose films for photonic applications. Adv. Mater. **30**: e1705948. DOI: 10.1002/adma.201705948.
41. Guo, S., Kamite, H., Suzuki, N., et al. (2018). Ambidextrous chirality transfer capability from cellulose tris(phenylcarbamate) to nonhelical chainlike luminophores: Achiral solvent-driven helix-helix transition of oligo- and polyfluorenes revealed by sign inversion of circularly polarized luminescence and circular dichroism spectra. Biomacromolecules **19**: 449–459. DOI: 10.1021/acs.biomac.7b01554.
42. Jarvis, M. (2003). Chemistry: Cellulose stacks up. Nature **426**: 611–612. DOI: 10.1038/426611a.
43. Klemm, D., Heublein, B., Fink, H.P., et al. (2005). Cellulose: Fascinating biopolymer and sustainable raw material. Angew. Chem. Int. Ed. **44**: 3358–3393. DOI: 10.1002/anie.200460587.
44. Hillmyer, M.A. (2017). The promise of plastics from plants. Science **358**: 868–870. DOI: 10.1126/science.aao6711.
45. Fox, S.C., Li, B., Xu, D., and Edgar, K.J. (2011). Regioselective esterification and etherification of cellulose: a review. Biomacromolecules **12**: 1956–1972. DOI: 10.1021/bm200260d.
46. You, J., Zhang, X., Mi, Q., et al. (2022). Mild, rapid and efficient etherification of cellulose. Cellulose **29**: 9583–9596. DOI: 10.1007/s10570-022-04879-x.
47. Zhang, X., Cheng, Y., You, J., et al. (2022). Ultralong phosphorescence cellulose with excellent anti-bacterial, water-resistant and ease-to-process performance. Nat. Commun. **13**: 1117. DOI: 10.1038/s41467-022-28759-x.
48. Khoshnevisan, K., Maleki, H., Samadian, H., et al. (2018). Cellulose acetate electrospun nanofibers for drug delivery systems: Applications and recent advances. Carbohydr. Polym. **198**: 131–141. DOI: 10.1016/j.carbpol.2018.06.072.
49. Vatanpour, V., Pasaoglu, M.E., Barzegar, H., et al. (2022). Cellulose acetate in fabrication of polymeric membranes: A review. Chemosphere **295**: 133914. DOI: 10.1016/j.chemosphere.2022.133914.
50. Oprea, M., and Voicu, S.I. (2023). Cellulose acetate-based materials for water treatment in the context of circular economy. Water **15**: 1860. DOI: 10.3390/w15101860.
51. Zhou, Q., Liu, M., Zhang, Y., et al. (2022). Packing density-promoted emission strategy toward tunable photoluminescence and room-temperature phosphorescence. ACS Sustainable Chem. Eng. **10**: 8568–8576. DOI: 10.1021/acssuschemeng.2c01953.
52. Jin, K., Song, G., Diao, H., et al. (2023). Hydrogen-bond assisted nonconventional photoluminescence of crystalline and amorphous cellulose. Cellulose **30**: 8139–8150. DOI: 10.1007/s10570-023-05392-5.
53. Hirata, S., and Vacha, M. (2016). Circularly polarized persistent room-temperature phosphorescence from metal-free chiral aromatics in air. J. Phys. Chem. Lett. **7**: 1539–1545. DOI: 10.1021/acs.jpclett.6b00554.
54. Li, M., Li, S.H., Zhang, D., et al. (2018). Stable enantiomers displaying thermally activated delayed fluorescence: efficient oleds with circularly polarized electroluminescence. Angew. Chem. Int. Ed. **57**: 2889–2893. DOI: 10.1002/anie.201800198.
55. Liang, X., Liu, T.T., Yan, Z.P., et al. (2019). Organic room-temperature phosphorescence with strong circularly polarized luminescence based on paracyclophanes. Angew. Chem. Int. Ed. **58**: 17220–17225. DOI: 10.1002/anie.201909076.
56. Wu, X., Huang, C.Y., Chen, D.G., et al. (2020). Exploiting racemism enhanced organic room-temperature phosphorescence to demonstrate Wallach's rule in the lighting chiral chromophores. Nat. Commun. **11**: 2145. DOI: 10.1038/s41467-020-15976-5.
57. Li, H., Li, H., Wang, W., et al. (2020). Stimuli-responsive circularly polarized organic ultralong room temperature phosphorescence. Angew. Chem. Int. Ed. **59**: 4756–4762. DOI: 10.1002/anie.201915164.
58. Liu, R., Ding, B., Liu, D., et al. (2021). Switchable circularly polarized room-temperature phosphorescence based on pure organic amorphous binaphthyl polymer. Chem. Eng. J. **421**: 129732. DOI: 10.1016/j.cej.2021.129732.
59. An, S., Gao, L., Hao, A., et al. (2021). Ultraviolet light detectable circularly polarized room temperature phosphorescence in chiral naphthalimide self-assemblies. ACS Nano **15**: 20192–20202. DOI: 10.1021/acsnano.1c08182.
60. Bai, X., Sun, Y., Jiang, Y., et al. (2021). Circularly polarized luminescence from solvent-free chiral organic pi-liquids. Angew. Chem. Int. Ed. **60**: 3745–3751. DOI: 10.1002/anie.202013550.
61. Li, H., Gu, J., Wang, Z., et al. (2022). Single-component color-tunable circularly polarized organic afterglow through chiral clusterization. Nat. Commun. **13**: 429. DOI: 10.1038/s41467-022-28070-9.
62. Wang, T., Liu, M., Feng, W., et al. (2023). Long - lived charge separation induced organic long - persistent luminescence with circularly polarized characteristic. Adv. Opt. Mater. **11**: 2202613. DOI: 10.1002/adom.202202613.
63. Liao, X.J., Pu, D., Yuan, L., et al. (2023). Planar chiral multiple resonance thermally activated delayed fluorescence materials for efficient circularly polarized electroluminescence. Angew. Chem. Int. Ed. **62**: e202217045. DOI: 10.1002/anie.202217045.
64. Ma, S., Ma, H., Yang, K., et al. (2023). Intense circularly polarized fluorescence and room-temperature phosphorescence in carbon dots/chiral helical polymer composite films. ACS Nano **17**: 6912–6921. DOI: 10.1021/acsnano.3c00713.
65. Guang, L., Lu, Y., Zhang, Y., et al. (2024). Circularly polarized phosphorescence of benzils achieved by chiral supramolecular polymerization. Angew. Chem. Int. Ed. **63**: e202315362. DOI: 10.1002/anie.202315362.
66. Xu, D., Liu, C., Li, H., et al. (2024). Circularly polarized room temperature phosphorescence of chiral bromoxanthone using a chiral self - assembled liquid crystal polymer frameworks. Adv. Opt. Mater. **63**: 2303019. DOI: 10.1002/adom.202303019.
67. Kamide, K., Miyamoto, I., and Okajima, K. (1993). Formation and properties of the lyotropic mesophase of the cellulose/mixed inorganic acid system. Polym. J. **25**: 453–461. DOI: 10.1295/polymj.25.453.
68. Kondo, T. (1997). The assignment of IR absorption bands due to free hydroxyl groups in cellulose. Cellulose **4**: 281–292. DOI: 10.1023/a:1018448109214.
69. Popescu, C.M., Popescu, M.C., and Vasile, C. (2011). Structural analysis of photodegraded lime wood by means of FT-IR and 2D IR correlation spectroscopy. Int. J. Biol. Macromol. **48**: 667–675. DOI: 10.1016/j.ijbiomac.2011.02.009.
70. Liang, Y.C., Cao, Q., Liu, K.K., et al. (2021). Phosphorescent carbon-nanodots-assisted forster resonant energy transfer for achieving red afterglow in an aqueous solution. ACS Nano **15**: 16242–16254. DOI: 10.1021/acsnano.1c05234.
71. Jin, K., Ji, X., Zhang, J., et al. (2022). Colourful organic afterglow materials with super-wide color gamut and scaled processability from cellulose. Mater. Today Chem. **26**: 101179. DOI: 10.1016/j.mtchem.2022.101179.

FUNDING AND ACKNOWLEDGMENTS

This work was supported by the National Natural Science Foundation of China (No. 52173292), and the Youth Innovation Promotion Association CAS (No. 2018040). The funders had no role in study design, data collection and analysis, decision to publish or preparation of the manuscript.

AUTHOR CONTRIBUTIONS

K.F.J. and J.M.Z. conceived the idea. K.F.J. performed the experiments. C.C.Y., J.X.Y., H.L.D., J.F.W. and K.K.Z. offered help to K.F.J. for the experiments. K.F.J., J.M.Z. and J.Z. discussed the results and wrote the manuscript.

DECLARATION OF INTERESTS

The authors declare no competing interests.

DATA AND CODE AVAILABILITY

The authors declare that the main data supporting the findings of this study are available within the paper and its Supplementary information. Extra data are available on reasonable request from the corresponding author.

SUPPLEMENTAL INFORMATION

It can be found online at https://doi.org/10.59717/j.xinn-mater.2024.100096